Fabrication of low loss polymer inverse ridge waveguide using inductively coupled plasma etching

Xiaoqiang Sun (孙小强), Kun Zhang (张 琨), Changming Chen (陈长鸣), Xiaodong Li (李晓东), Fei Wang (王 菲), and Daming Zhang (张大明)*

State Key Laboratory on Integrated Optoelectronics, Jilin University, Changchun 130012, China

**Corresponding author: zhangdm@jlu.edu.cn*

Received August 15, 2011; accepted November 4, 2011; posted online May 16, 2012

The optimized oxygen inductively coupled plasma etching parameters are systematically studied to fabricate Poly (methyl-methacrylate-glycidly-methacrylate) inverse ridge waveguide with smooth vertical features. The etch rate, surface roughness and vertical profile are characterized by atomic force microscopy and scanning electron microscopy. The optimized etching parameters are found to be 400-W antenna-RF power, 30-W radio frequency (RF) bias power, 1-Pa-chamber pressure, and 40-sccm be O_2-flow rate. Spin-coating butyl acetate diluted polymer solution onto the channel waveguide is proved to be an effective method which can decrease the surface roughness. According the results, the RMS rouqhness of the film decreases 80%. Optical propagation loss can be reduced from 2.6 to 1.5 dB/cm for the above reason.

OCIS codes: 220.0220, 130.0130, 230. 0230.

doi: 10.3788/COL201210.S12202.

Potential applications of polymer waveguides in optical communications, micromachining, and sensors have attracted much attention for the merits of easy fabrication, controllable refractive index, good thermal stability and low optical loss[1−6]. As a key issue of polymer waveguides, optical loss may be caused by different factors, including intrinsic material-absorption, mismatching of modes and optical scattering due to waveguide roughness formed in the process of etching[7−9]. The etching process has been intensively studied because it will affect waveguide figure and optical loss remarkably. For example, the organic/inorganic hybrid material of Er-Yb doped SU-8 applied in optical amplifier is hard to etch, so an inverse ridge waveguide which adopts channel structure is adopted to ease device fabrication[10]. Different processing technologies, including spin-coating, photolithography of patterning the etch mask, ion etching or electron-beam direct writing of waveguide structure are adopted in the fabrication of polymer waveguides[11−13]. Since both isotropic etching by chemical reaction and anisotropic etching by ionic bombardment will happen in the plasma-etching process, etching parameters must be optimized to obtain smooth vertical profile, which is in favor of reducing optical loss[14−17]. As an effective method, reactive ion etching (RIE) has been well studied and used in polymer waveguide fabrication[18]. How ever , the ion density and the kinetic energy in RIE process can not be regulated individually because they are both controlled by one radio-frequency (RF) power. In contrast, for inductively coupled plasma (ICP) etching, the ion density and the kinetic energy can be regulated by two independent RF power sources, respectively. ICP etching can generate high-density plasmas ($>10^{11}$ cm^{-3}), which is more suitable for submicron and uniform process. Therefore, this method can provide smoother sidewall, higher etch rate and anisotropic etching than RIE approach[19]. In this letter, parameters of ICP etching are systematically studied and optimized for Poly(methyl-methacrylate-glycidly-methacrylate) (P(MMA-GMA)) inverse ridge waveguide fabrication. The etch rate, vertical profile and surface roughness of P(MMA-GMA) channel are investigated as a function of antenna RF power, bias RF power, chamber pressure, or O_2 flow rate. Spin-coating dilute polymer solution onto the channel waveguide is proved to be an effective method to smooth the film surface and reduce optical loss.

The P(MMA-GMA) polymer material synthesized by ourselves is used in this study due to its stable chemical properties and good optical characteristics. Its molecular structure is shown in Fig. 1. The refractive index (RI) of P(MMA-GMA) is about 1.48 at wavelength of 1 550 nm. The bis-A-epoxy is adopted as the RI regulator for P(MMA-GMA) to form the specific RI difference of 0.01. Then it can be used both as the core and the cladding material. The root-mean-square (RMS) roughness of P(MMA-GMA) film is 0.32 nm for an area of 20 μm^2.

To investigate the affects of ICP etching on optical

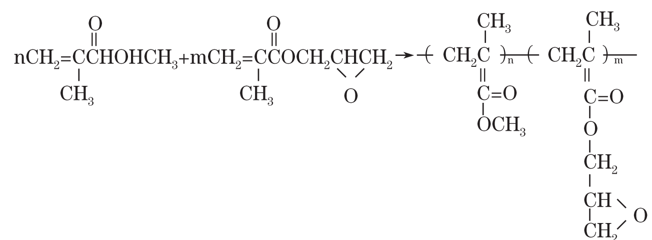

Fig. 1. Molecular structure of P(MMA-GMA).

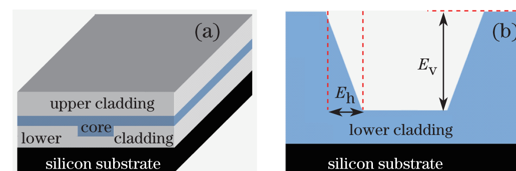

Fig. 2. (a) Schematic diagram of inverse ridge waveguide structure and (b) anisotropy etching of channel on lower cladding.

 © 2012 Chinese Optics Letters

loss, an inverse ridge waveguide is fabricated. Figure 2(a) presents the schematic diagram of the inverse ridge waveguide. The anisotropy of the etch profile is given by

$$A = 1 - (E_h/E_v), \quad (1)$$

where E_h is the horizontal etch depth and E_v is the vertical etch depth, as shown in Fig. 2(b). A larger anisotropy of A presents a more vertical profile.

The fabrication process of the inverse ridge waveguide is as follows: firstly, P(MMA-GMA) lower cladding was spin-coated onto the cleaned silicon substrate at 2 500 rpm and baked at 120°C for 2.5 hours for removing the residual solvent. A layer of 100-nm-thick aluminum was thermal evaporated onto the top of P(MMA-GMA) as the metal mask. To define the channel patterns on the aluminum film, BP212 photoresist was spin-coated onto the metal film and patterned by traditional photolithography. Then, oxygen etching of P(MMA-GMA) was carried out under different powers and pressures with an ICP system of CE-300I (ULVAC, Japan). The He-cooling system kept the temperature of the lower electrode at 20 °C. The etch rate, surface roughness and vertical profile are evaluated as functions of antenna RF power, bias RF power, chamber pressure and O_2 flow rate. To obtain smooth vertical waveguide, the above parameters are optimized under the condition that one parameter is changed while the other parameters are fixed.

To investigate the effects of antenna RF power, it was increased from 200 to 500 W when the other parameters were fixed at 30-W-bias-RF power, 0.5-Pa-chamber pressure, and 40-sccm-O_2-flow rate. The etch rate, RMS and vertical profile as functions of antenna RF power is shown Fig. 3. As shown in Fig. 3, the etch rate increases from 0.34 to 1.00 μm/min when the antenna RF power grows up from 200 to 500 W. It means that the antenna RF power plays an important role for the generation of reactive radicals and ionic species, and directly affects the plasma density. Since the increment of plasma density will enhance chemical etching, the RMS roughness of the film decreases from 22.4 to 13.1 nm, which is favorable to reduce scattering loss. The anisotropy of channel waveguide after ICP etching under different antenna RF powers is defined by A. It increases from 0.857 to 0.965 with the increasing of antenna RF power. From the experimental results, trapezoidal figure appeares when power was lower than 400 W. Moreover, the higher antenna RF power of 500 W leads to undercut and an overhang of the metal mask above the P(MMA-GMA) channel edge because of the high plasma density. So, an antenna RF power of 400 W is more preferable to obtain smoother vertical profile.

To evaluate the effect of bias RF power on ICP etching, the power is increased from 15 to 60 W as the other parameters are fixed at 400-W-antenna-RF power, 0.5-Pa-chamber pressure, and 40-sccm-O_2-flow rate. As shown in Fig. 4, the etch rate increases from 0.52 to 1.65 μm/min. Since the etch rate scales up almost three times, the bias RF power is convinced to be the main factor to accelerate etch rate. Meanwhile, the RMS roughness significantly increases from 8.1 to 41 nm. As we know, the plasma energy determined by bias RF power controls the directional movement and physical bombardment of ions in ICP etching. Therefore, the surface roughness is proved to be strongly depending on the plasma bombardment, which will be enhanced at higher bias RF power. Though low bias power is good for obtaining smoother surface, it can weaken the directionality of plasma movement. Moreover, the isotropic etching by chemical reaction can predominate over anisotropic etching which results in undesired undercut at low bias power. Therefore, according to values of A in Fig. 4, the best vertical edge appears under bias RF power of 30 W Based on trigonometric function calculation, the sidewall vertical angle of the inverse ridge waveguide is less than 4°, so 30-W-bias-RF power is the best choice to achieve smooth vertical profile.

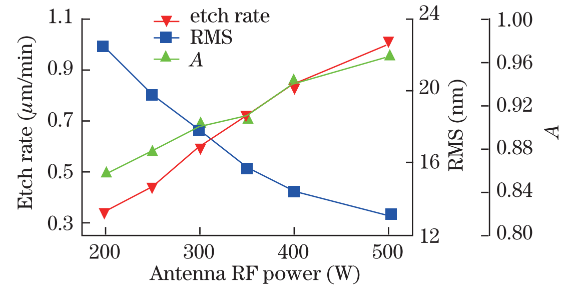

Fig. 3. Etch rate, surface roughness and anisotropy as functions of antenna RF power at 30-W-bias-RF power, 40-sccm-O_2-flow rate, and 0.5-Pa-chamber pressure.

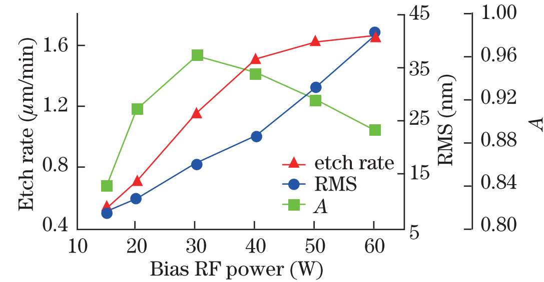

Fig. 4. Etch rate, surface roughness and anisotropy as functions of bias RF power at 400-W-RF-bias power, 40-sccm-O_2-flow rate, and 0.5-Pa-chamber pressure.

To investigate the effect of chamber pressure on ICP etching, the antenna RF power, bias RF power and O_2 flow rate are set to 400 W, 30 W, and 40 sccm, respectively. As shown in Fig. 5, the etch rate increases from 0.72 to 0.85 μm/min as the chamber pressure grows up from 0.5 to 1 Pa, and reduces to 0.63 μm/min when the chamber pressure increases from 1 to 5 Pa. The etch rate has a maximum in the process of pressure increment. This can be explained that ICP etching is enhanced when the chamber pressure is lower than 1 Pa due to the increasing of gas molecules and dissociated plasmas. However, the amount of reactive species and the etch rate will change to be determined by antenna RF power when the pressure is greater than 1 Pa. And the kinetic energy of plasma decreases due to the shortening of the mean free path, which leads to the etch rate dropping in Fig. 5. As shown in Fig. 5, the roughness increases from 11.8 to 22.3 nm as the chamber pressure grows up from 0.5 to 5 Pa, which can be attributed

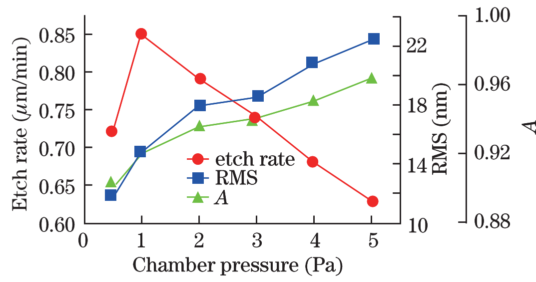

Fig. 5. Etch rate, surface roughness and anisotropy as functions of chamber pressure at 400-W-antenna-RF power, 30-W-RF-bias power, and 40-sccm-O_2-flow rate.

As we know, the distance between the collisions of plasmas is closely related to the incident angles. The roughness change measured can be explained by the oxygen plasma incident angles on the polymer film surface, and the subsequent oxygen gas flow redistribution due to the local morphological features. If no reaction occurs on the first hit between the oxygen plasma and P(MMA-GMA) film, the plasma will move towards the valleys on the film surface. This leads to more serious local etching of the valleys compared to the peaks. At lower chamber pressure, plasmas are incident at larger oblique angles, which is in favor of obtaining smoother surface. Vertical profile of the channel is clearly demonstrated by variation of A in Fig. 5. According to the above analysis, the incident angles of plasmas on the sidewall are becoming normal at higher pressure, which will induce a trapezial figure. In contrast, the plasmas flux is almost vertically incident on the film at lower pressure. So, the chamber pressure of 1 Pa is more preferable.

The flow rate of O_2 is changed from 20 to 60 sccm when the other parameters were fixed at 1-Pa-chamber pressure, 400-W-antenna-RF power, 30-W-bias-RF power to study the effects of gas flow rate. Fig. 6 shows the variations of etch rate and surface roughness as functions of O_2 flow rate. The etch rate increases from 0.61 to 0.98 μm/min due to the increment of plasma densities and enhancement of the chemical etching effect. However the flow rate growing diminished the mean free path and directional movement of oxygen plasmas, so larger flow rate will not speed up the removal of the substrate polymer molecules remarkably. The etch rate becomes saturated as the O_2 flow rate is larger than 40 sccm. For the same reason, the RMS roughness decreases from 19.5 to 12.5 nm. A in Fig. 6 illustrates the vertical profiles of channel waveguide after plasma etching.

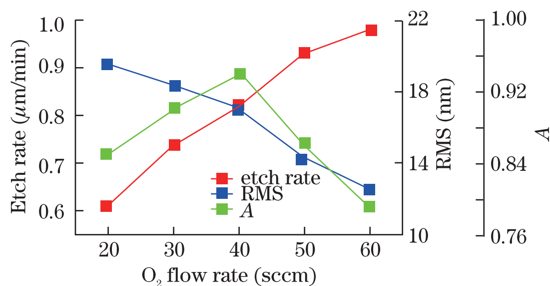

Fig. 6. Etch rate, surface roughness and anisotropy as functions of O_2 flow rate at 1-Pa-chamber pressure, 400-W-ICP power, and 30-W-RF-bias power.

to chamber pressure induced bias RF power increasing. As shown in the Fig. 6, no obvious isotropic etching is observed at different O_2 flow rate, but the trapezium emerges due to the attenuation of anisotropic etching with the increment of plasma density at O_2 flow rate of 50 sccm. Therefore, 40 sccm is more favorable to obtain smooth vertical waveguide.

According to the above analysis, the optimized etching parameters are as follows: 400-W-antenna-RF power, 30-W-bias-RF power, 1-Pa-chamber pressure, 40-sccm-O_2-flow rate. Figure 7 shows the SEM image of P(MMA-GMA) channel waveguide after ICP etching.

As shown in Fig. 7, though the channel has vertical edge, the RMS roughness of the channel bottom is still relatively high. This roughness will induce extra scattering loss and hinder mode field propagation. A method of steam-redissolution technique once was used to decrease sidewall scattering loss of polymer waveguide[20], but the waveguide needs to be placed in a high temperature and saturated steam atmosphere by this approach. It will damage the figure of waveguide edge. So directly spin-coating diluted P(MMA-GMA) solution onto the channel waveguide surface is proposed by us to lower the bottom and sidewall roughness. Firstly, the concentration of P(MMA-GMA) solution is diluted by butyl acetate for 500 times. According to the measurement of surface profile measuring system, the thickness of the diluted film was found to be about 43 nm. Then the same molecules can be absorbed and got into the bottom of the channel after spin-coating. Figure 8 demonstrates the SEM images of film surface before and after spin-coating diluted P(MMA-GMA) solution. The height and density of tree-like protrusion reduced obviously. The RMS roughness of the film decreased 80%, which reduced from 12.8 to 2.51 nm. To evaluate the validity of this method, the inverse ridge waveguide with P(MMA-GMA) as core and cladding layers is used to study the optical loss. The optical propagation loss of optimized straight waveguide is obtained by butt-coupling method. Compared to waveguide with no diluted P(MMA-GMA) layer, the propagation loss decreases 42% from 2.6 to 1.5 dB/cm.

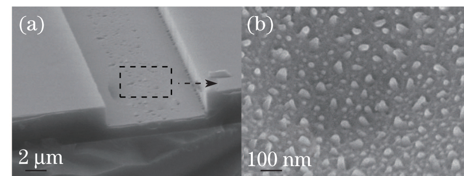

Fig. 7. SEM images of P(MMA-GMA) channel fabricated with optimized parameters. (a) P(MMA-GMA) channel after ICP etching; (b) local region on the bottom of channel.

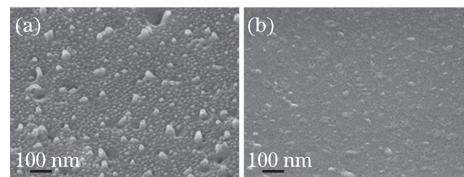

Fig. 8. SEM images of film surface roughness change (a) before and (b) after spin-coating diluted P(MMA-GMA) solution.

In conclusion, a P(MMA-GMA) inverse ridge waveguide structure is proposed in this letter. The oxygen ICP etching conditions are investigated and optimized for the fabrication of smooth vertical inverse ridge waveguide. AFM and SEM images are used to characterize the etch rate, surface roughness and vertical profile of the waveguide. Experimental results show that spin-coating diluted P(MMA-GMA) solution onto the same material channel can decrease optical propagation loss of 1.1 dB/cm. We believe that this approach has great potential to effectively reduce scattering loss of polymer waveguide.

This work was supported by the National Natural Science Foundation of China (Nos. 61077041, 61177027, 61107109, and 60807029), the Science and Technology Foundation of Jilin Province, China (Nos. 20090352, 20100174, and 20110315), and the Program for Special Funds of Basic Science & Technology of Jilin University (Nos. 200905005, 201100253, and 201103071).

References

1. K. Iiyama, T. Ishida, Y. Ono, T. Maruyama, and T. Yamagishi, IEEE Photon. Technol. Lett. **23,** 275 (2011).
2. S. Li, Q. Lin, L. Chen, and X. Wu, Chin. Opt. Lett. **9,** 081302 (2011).
3. N. Bamiedakis, J. Beals, R. V. Penty, I. H. White, J. V. Degroot, and T. V. Clapp, IEEE J. Quantum Electron. **45,** 415 (2009).
4. J. Kobayashi, T. Matsuura, Y. Hida, S. Sasaki, and T. Maruno, J. Lightwave Technol. **16,** 1024 (1998).
5. B. L. Booth, J. Lightwave Technol. **7**, 1445 (1989).
6. F. Wang, W. Sun, A. Li, M. Yi, Z. Jiang, and D. Zhang, Chin. Opt. Lett. **3,** 568 (2004).
7. M. H. Ibrahim, N. M. Kassim, A. B. Mohammad, and A. S. M. Supa'at, Optoelectronics and Advanced Materials-rapid Communications **3,** 917 (2009).
8. J. Lin, A. Leven, R. Reyes, Y. K. Chen, and F. S. Choa, J. Vac. Sci. Technol. B **23,** 1361 (2005).
9. Y. Wang, Z. Lin, X. Cheng, C. Zhang, F. Gao, and F. Zhang, Appl. Phys. Lett. **85,** 3995 (2004).
10. C. Chen, D. Zhang, T. Li, D. Zhang, L. Song, and Z. Zhen, J. Nanosci. Nanotechnol. **10,** 1947 (2010).
11. S. Lu, Y. Yan, G. Jin, W. H. Wong, and E. Y. B. Pun, Chin. Opt. Lett. **2,** 362 (2004).
12. Y. Zhao, D. Zhang, F. Wang, Z. Cui, M. Yi, C. Ma, W. Guo, and S. Liu, Opt. Laser Technol. **36,** 657 (2004).
13. M. A. Uddin, H. P. Chan, C. K. Chow, and Y. C. Chan, J. Electron. Mater. **33,** 224 (2004).
14. B. Schuppert, E. Brose, R. Moosburger, and K. Petermann, J. Vac. Sci. Technol. A **18,** 385 (2000).
15. N. Agarwal, S. Ponoth, J. Plawsky, and P. D. Persans, J. Vac. Sci. Technol. A **20,** 1587 (2002).
16. J. H. Kim, E. J. Kim, H. C. Choi, C. W. Kim, J. H. Cho, Y. W. Lee, B. G. You, S. Y. Yi, H. J. Lee, K. Han, W. H. Jang, T. H. Rhee, J. W. Lee, and S. J. Pearton, Thin Solid Films **341,** 192 (1999).
17. Y. Wang, Z. Lin, C. Zhang, F. Gao, and F. Zhang, IEEE J. Sel. Topics Quantum Electron. **11,** 254 (2005).
18. Y. Zhao, F. Wang, Z. Cui, J. Zheng, H. Zhang, D. Zhang, S. Liu, and M. Yi, Microelectron. J. **35,** 605 (2004).
19. K. Han, J. Kim, and W.-H. Jang, J. Appl. Poly. Sci. **79,** 176 (2001).
20. H. Zhang, C. Ma, Z. Qin, X. Zhang, D. Zhang, S. Liu, and D. Zhang, Acta Opt. Sin. (in Chinese) **27,** 690 (2007).